Dynamic pneumococcal genetic adaptations support bacterial growth and inflammation during coinfection with influenza

Amanda P. Smith[a], Lindey C. Lane[a], Tim van Opijnen[b], Stacie Woolard[c], Robert Carter[d], Amy Iverson[e], Corinna Burnham[e], Peter Vogel[f], Dana Roeber[g], Gabrielle Hochu[a], Michael D.L. Johnson[h], Jonathan A. McCullers[a], Jason Rosch[e]#, Amber M. Smith[a]#

[a]Department of Pediatrics, University of Tennessee Health Science Center, Memphis, TN, USA

[b]Department of Biology, Boston College, Chestnut Hill, MA, USA

[c]Departments of Flow Cytometry, St. Jude Children's Research Hospital, Memphis, TN, USA

[d]Departments of Oncology, St. Jude Children's Research Hospital, Memphis, TN, USA

[e]Departments of Infectious Diseases, St. Jude Children's Research Hospital, Memphis, TN, USA

[f]Departments of Pathology, St. Jude Children's Research Hospital, Memphis, TN, USA

[g]The Hartwell Center, St. Jude Children's Research Hospital, Memphis, TN, USA

[h]Department of Immunobiology, University of Arizona, Tucson, AZ, USA

Address correspondence to amber.smith@uthsc.edu , jason.rosch@stjude.org

Abstract

Streptococcus pneumoniae (pneumococcus) is one of the primary bacterial pathogens that complicates influenza virus infections. These bacterial coinfections increase influenza-associated morbidity and mortality through a number of immunological and viral-mediated mechanisms, but the specific bacterial genes that contribute to post-influenza pathogenicity are not known. Here, we used genome-wide transposon mutagenesis (Tn-Seq) to reveal bacterial genes that confer improved fitness in influenza-infected hosts. The majority of the 32 identified genes are involved in bacterial metabolism, including nucleotide biosynthesis, amino acid biosynthesis, protein translation, and membrane transport. We generated single-gene deletion (SGD) mutants of five identified genes: SPD1414, SPD2047 (*cbiO1),* SPD0058 (*purD*), SPD1098, and SPD0822 (*proB*), to investigate their effect on *in vivo* fitness, disease severity, and host immune responses. Growth of SGD mutants was slightly attenuated *in vitro* and *in vivo*, but each still grew to high titers in the lungs of mock- and influenza-infected hosts. Despite high bacterial loads, mortality was significantly reduced or delayed with all SGD mutants. Time-dependent reductions in pulmonary neutrophils, inflammatory macrophages, and select proinflammatory cytokines and chemokines were also observed. Immunohistochemical staining further revealed that neutrophil phenotype and distribution was altered in the lungs of influenza-SGD coinfected animals. These studies demonstrate a critical role for specific bacterial genes and for bacterial metabolism in driving virulence and modulating immune function during influenza-associated bacterial pneumonia.

Introduction

Bacterial pathogens often complicate influenza virus infections, causing increased morbidity and mortality, and *Streptococcus pneumoniae* (pneumococcus) is one of the leading pathogens that has presented as a risk factor for hospitalization, severe disease, and mortality during infuenza epidemics and pandemics (1-7). There is considerable genetic diversity within and between pneumococcal serotypes, and laboratory and clinical studies suggest that specific strains are preferentially promoted in influenza-infected hosts (8-10). Despite the clinical importance of the synergy between influenza viruses and pneumococci, a systematic investigation into bacterial factors that contribute to coinfection disease severity has yet to be performed.

During influenza A virus (IAV) coinfection with pneumococcus, bacteria are able to grow rapidly, viral burden increases, and significant inflammation amasses. The host-pathogen interplay is complex with numerous factors contributing to pathogen growth and host disease. Several studies have investigated the impact of viral virulence factors (e.g., reduced epithelial integrity, PB1-F2, viral neuraminidase (NA)), bacterial virulence factors (e.g., bacterial NA, enhanced attachment, sialic acid catabolism), and host immune responses (e.g., cytokine storm, cell dysfunction and death) on the pathogenicity of bacterial coinfections during influenza virus infection (11-17). Incidence and severity of coinfection is, in part, a function of the detrimental effects that influenza virus infection has on key immune responses (e.g., alveolar macrophages (AMΦ) depletion and dysfunction (18-23), neutrophil and inflammatory macrophage dysfunction (23-32), and

abundant production of pro-inflammatory cytokines (12-17, 33)). However, the role that single genes play in pathogenicity during coinfection remains unclear.

Pneumococci, in particular, are highly adaptable and alter gene expression and metabolic functions to adjust to multiple host niches during infection and several genes have been identified as regulators of transmissibility and disease severity during primary pneumococcal infection (34-45). Select pneumococcal virulence factors have been investigated in the context of IAV infection (e.g., sialic acid catabolism) (46-49), but systematic genomic screens have not yet been employed to assess pneumococcal adaptations during IAV-pneumococcal coinfection. Genome-wide screens have been used to identify influenza-induced changes during *Haemophilus influenzae* coinfection (50), which included changes in purine biosynthesis, amino acid metabolism, iron homeostasis, and cell wall synthesis (50). Genomic screens assessing pneumococcal adaptations of the TIGR4 strain in hosts with sickle cell anemia suggested genes involved in purine biosynthesis, complement function, and iron acquisition were of importance (51). Given these findings and the similarities in bacterial metabolic adaptations under various host pressures, understanding how bacterial genes influence influenza-pneumococcal coinfection is imperative.

Here, we used genome-wide transposon insertion sequencing (Tn-Seq) (52) to investigate all non-essential pneumococcal genes that modulate disease severity and immune responses. Doing so could help establish important species- and strain-dependent and independent mechanisms amenable to targeting with therapeutics. Our

Tn-Seq screen revealed 32 total genes, some with known metabolic functions, that confer bacterial fitness during influenza-pneumococcal coinfection compared to primary bacterial infection. Interestingly, there were time-dependent differences. To determine how select genes affect pathogenicity and host immune responses, we generated 5 single-gene deletion (SGD) mutants (D39Δ*cbiO1* (SPD2047), D39Δ*purD* (SPD0058), D39Δ*1414*, D39Δ*1098*, and D39Δ*proB* (SPD0822)). Lethality was significantly reduced or eliminated during infection in infected animals despite high bacterial loads in the lungs and blood. This was concurrent with significant reductions in innate pulmonary immune responses and development of pneumonia in IAV-infected animals. Taken together, these data indicate a critical role for pneumococcal metabolism in shaping host responses and altering disease severity during post-influenza bacterial pneumonia.

Results

Bacterial Adaptations During Pneumococcal Coinfection With Influenza

To identify the pneumococcal factors that increase bacterial fitness during IAV infection, we employed a high-throughput, transposon sequencing (Tn-Seq) approach (52). We generated a library of ~50,000 transposon insertion mutants in the type 2 pneumococcal strain D39, then infected groups of mice with 75 $TCID_{50}$ (50% tissue culture infectious dose) influenza A/Puerto Rico/34/8 (PR8) or mock control (PBS) followed 7 d later with 10^6 CFU (colony forming units) of the transposon library. Bacteria were collected from lungs harvested at 12 h or 24 h post-bacterial infection (pbi), genomic DNA was isolated and sequenced, and the relative abundance and fitness of transposon mutants was calculated (Supplementary Information). In comparing the results from pre- and post-

infection and from mock- and IAV-infected animals, 17 genes conferred differential fitness at 12 h, and 23 genes had differential fitness at 24 h pbi. Of these, 8 genes were detected at both time points (Table 1, Fig 1).

The core set of genes identified at 12 h and 24 h pbi are responsible for amino acid biosynthesis, nucleotide biosynthesis, protein translation, and membrane transport (Fig 1). Genes in the purine biosynthesis pathway comprised the largest number of genes (8 total; SPD0002 (*dnaN*), SPD0052, SPD0053 (*purF*), SPD0054 (*purM*), SPD0055 (*purN*), SPD0057 (*purH*), SPD0058 (*purD*), and SPD0059 (*purE*)) followed by ATP-binding cassette (ABC) transporters (5 total; SPD1098, SPD1099, SPD2047 (*cbiO1)*, SPD2048 (*cbiO2*), and SPD1354 (putative)), protein translation (6 total; SPD0395 (*efp*), SPD1782 (*ksgA*), SPD0907 (hemK), SPD1130 (licD2), SPD1293, SPD1923), and proline biosynthesis (3 total; SPD0822 (*proB*), SPD0823 (*proA*), SPD0824 (*proC*)). Other genes included a putative membrane protein (SPD1090), carbon metabolism (SPD0723 (*ripA*), SPD1087, SPD1333 (putative), and SPD1468), and riboflavin metabolism (SPD0994).

Table 1: Pneumococcal Genes with Significant Differential Fitness During Coinfection with IAV. Pneumococcal fitness genes identified at 12 h and 24 h pbi by Tn-Seq during IAV infection compared to mock-infected hosts. Highlighted in bold are the genes chosen for additional characterization.

Locus	Gene	Description	12	24
SPD_0002	dnaN	DNA polymerase III subunit beta	√	
SPD_0052		phosphoribosylformylglycinamidine synthase, putative		√
SPD_0053	purF	amidophosphoribosyltransferase		√
SPD_0054	purM	phosphoribosylformylglycinamidine cyclo-ligase		√
SPD_0055	purN	phosphoribosylglycinamide formyltransferase	√	√
SPD_0057	purH	bifunctional purine biosynthesis protein PurH	√	√
SPD_0058	**purD**	**phosphoribosylamine--glycine ligase**	**√**	**√**
SPD_0059	purE	phosphoribosylaminoimidazole carboxylase, catalytic	√	√
SPD_0182		conserved hypothetical protein	√	
SPD_0372		sodium:alanine symporter	√	√
SPD_0395	efp	translation elongation factor P		√
SPD_0723	rpiA	ribose 5-phosphate isomerase A	√	
SPD_0822	**proB**	**glutamate 5-kinase**		**√**
SPD_0823	proA	gamma-glutamyl phosphate reductase		√
SPD_0824	proC	pyrroline-5-carboxylate reductase		√
SPD_0907	hemK	HemK protein	√	
SPD_0994	ribF	riboflavin biosynthesis protein RibF	√	
SPD_1087	fhs	formate--tetrahydrofolate ligase		√
SPD_1090		membrane protein, putative		√
SPD_1098		**amino acid ABC transporter, amino acid-binding**	**√**	**√**
SPD_1099		amino acid ABC transporter, ATP-binding protein		√
SPD_1130	licD2	phosphotransferase LicD2		√
SPD_1293		acetyltransferase, GNAT family protein		√
SPD_1309	pgdA	peptidoglycan GlcNAc deacetylase		√
SPD_1333		conserved hypothetical protein		√
SPD_1354		conserved hypothetical protein	√	
SPD_1414		**oxalate:formate antiporter**	**√**	**√**
SPD_1468		phosphoglycerate mutase	√	
SPD_1782	ksgA	dimethyladenosine transferase	√	
SPD_1923		2,3,4,5-tetrahydropyridine-2-carboxylate N-	√	
SPD_2047	**cbiO1**	**cobalt ABC transporter, ATP-binding protein**	**√**	**√**
SPD_2048	cbiO2	cobalt ABC transporter, ATP-binding protein CbiO2		√
Total			**17**	**23**

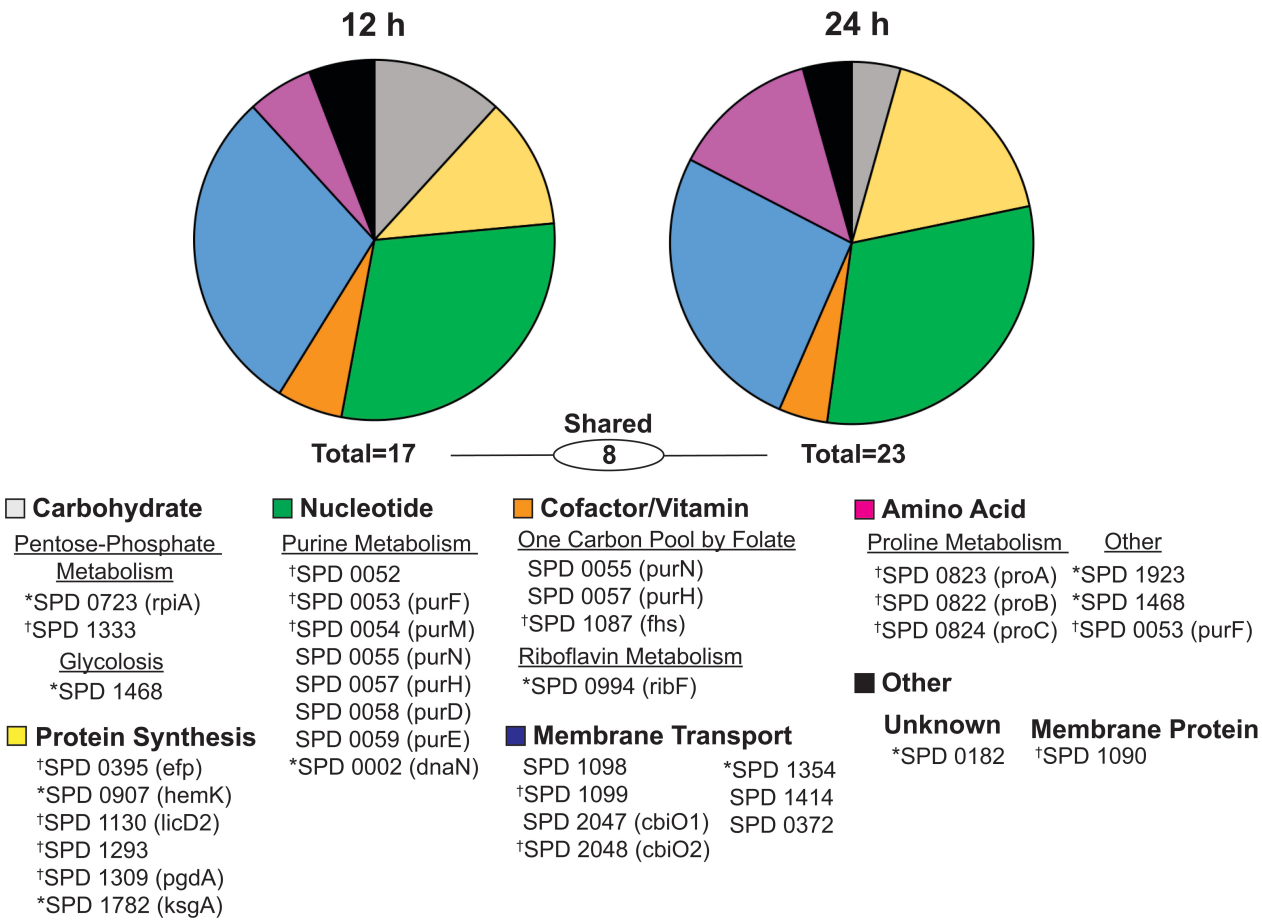

Fig 1: Time-Dependent Analysis of Pneumococcal Genes Impacting Fitness During Influenza Virus Coinfection. Functional breakdown of the pneumococcal genes that impact bacterial fitness during coinfection with influenza A virus as identified by Tn-Seq. Markers identify genes important at only *12 h pbi (17 total) or only at †24 h pbi (23 total). No marker indicates significance at both time points (8 total).

Impaired Bacterial Metabolism Selectively Reduces Fitness *In Vitro*

We generated single-gene deletion (SGD) bacterial mutants from 3 of the identified categories (D39Δ*cbiO1*, D39Δ*1414*, D39Δ*1098* (membrane transport), D39Δ*purD* (purine metabolism), and D39Δ*proB* (proline metabolism)) to assess the differential fitness of

genes predicted by Tn-seq (Table 1, Fig 1, and Table S1). Growth of the SGD mutants in culture medium was unaffected, with the exception of D39Δ*cbiO1*, which was significantly attenuated from 3 h to 8 h ($p<0.05$) and was the only SGD strain that had not autolysed after 24 h (Fig 2A). During metabolic starvation (i.e., PBS), D39Δ*1098* decayed more rapidly ($p=0.01$) and D39Δ*cbiO1* more slowly ($p<0.01$), but other SGD mutants were similar to WT (Fig 2B). Bacterial growth was rescued when PBS cultures were supplemented with lung homogenate supernatants (s/n) (Fig S1A-B) and was not different than WT D39 after 6 h of culture in lung homogenate s/n from mock- or IAV-infected mice (75 $TCID_{50}$ PR8, 7 d) (Fig S1C-D).

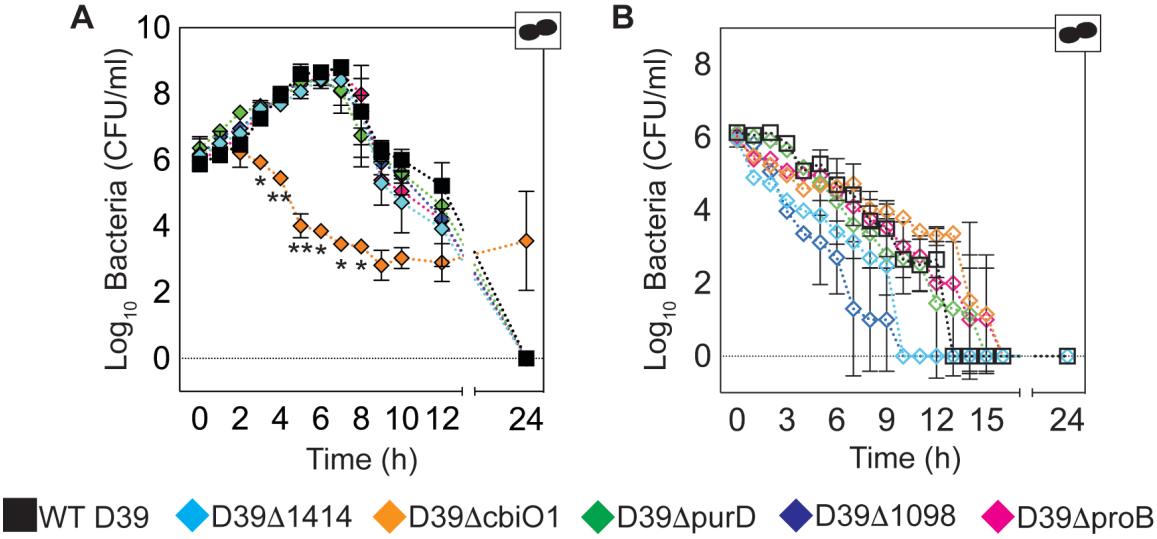

Fig 2: *In vitro* Growth Kinetics of SGD Mutant Bacteria. Bacteria were grown at 37°C in 1 ml of ThyB (A) or PBS (B). Signficance is indicated as *$p<0.05$ and **$p<0.01$ (D39Δ*cbiO1* only) compared to WT D39 at the indicated time point (Panel A). Each symbol (squares or diamonds) is the mean of two representative experiment and the bars are the geometric mean ± standard deviation (SD). Cartoons indicate pathogens in the culture (bacteria alone).

Impaired Bacterial Metabolism Protects Against Virulence *In vivo*

Reduced Mortality

To establish the effect of gene deletion on pathogenicity, weight loss was monitored as a measure of disease severity (Fig 3, Table S2). In mock- and IAV-infected animals, infection with WT D39 resulted in 100% mortality by 72 h pbi and 48 pbi, respectively (Fig 3A-B). In mock-infected animals, mortality was reduced by 90-100% in 4 out of 5 SGD mutants and by 40% with D39Δ*proB* (all $p<0.01$) (Fig 3A, Table S2). Correspondingly, weight loss was significantly reduced (48 h pbi; $p<0.05$) (Fig 3C). In IAV-infected animals, mortality was reduced by 40-90% in 4 out of 5 SGD mutants (all $p<0.01$) (Fig 3B, Table S2). Coinfection with D39Δ*proB* resulted in 100% mortality; however, the mean survival time was lengthened by 5 d ($p<0.01$) (Fig 3B, Table S2). In IAV-infected animals, weight loss was not significantly reduced compared to WT D39 (24 h pbi; $p>0.05$) (Fig 3D) and weights of all SGD-infected animals, except D39Δ*proB*, began to rebound ~3 d pbi and returned to baseline by 12-14 d pbi.

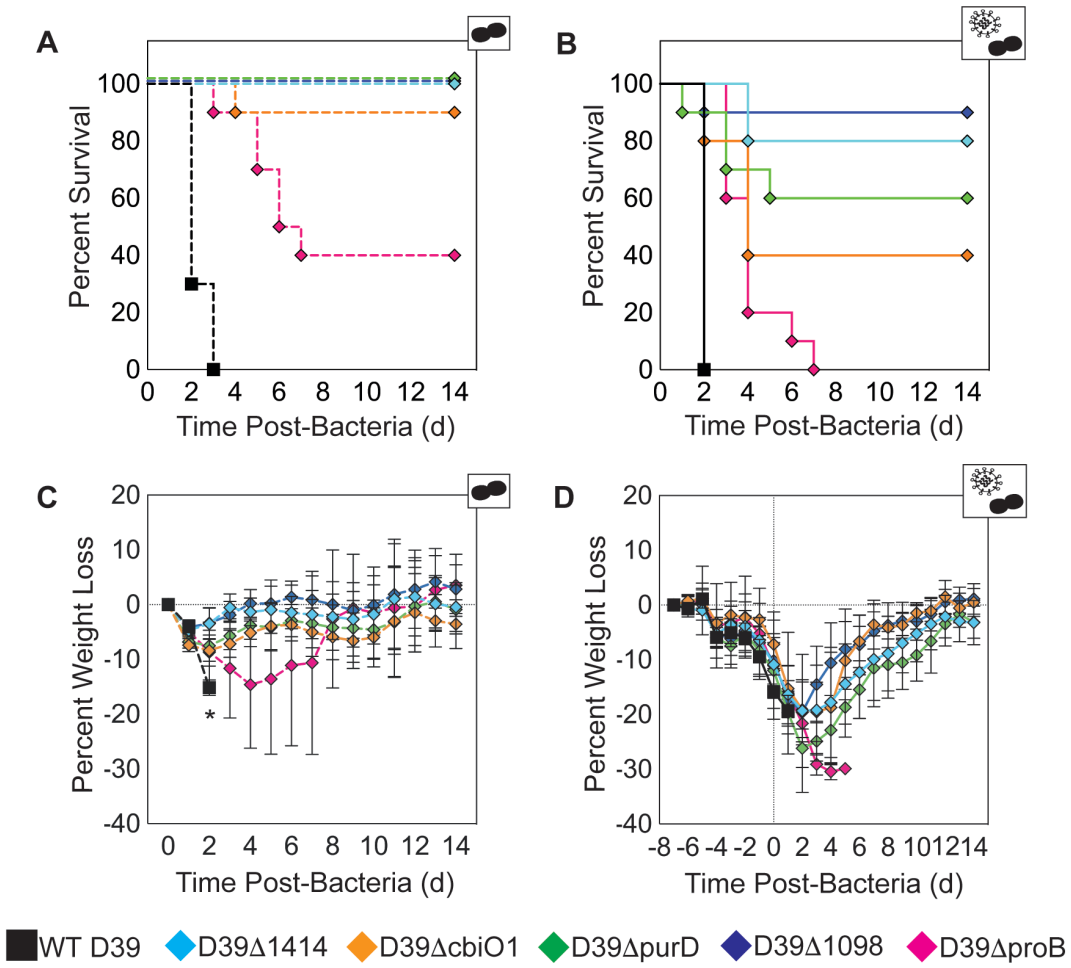

Fig 3: *In vivo* Pathogenicity of Infection with SGD Mutant Bacteria. Kaplan-Meier survival curves (A-B) and weight loss (percent loss compared to naïve) (C-D) of mice mock-infected (PBS) (dashed lines; Panel A, C) or IAV-infected (75 $TCID_{50}$ PR8) (solid lines; Panel B, D) followed 7 d later with 10^6 CFU of the indicated bacteria. Survival curves are significantly different ($p<0.01$) for each SGD mutant compared to WT D39, in mock- (Panel A) and IAV- (Panel B) infected animals. Differences in survival curves are detailed in Table S2**.** Signficant difference in weight loss is indicated as *$p<0.05$ for each SGD mutant (diamonds) compared to WT D39 (square) at the indicated time point (Panel C).

Data are shown as the mean ± standard deviation (SD) from 10 mice/group. Cartoons indicate infection status of study group (bacteria alone or virus plus bacteria).

Reduced Bacteria in the Lung and Blood

Lung titer kinetics of the SGD mutants *in vivo* (Fig 4A-B) mirrored *in vitro* titer kinetics in lung s/n supplemented cultures (Fig S2C-D). At 4 h pbi, SGD mutant lung titers were 0.6-1.4 $\log_{10}$ CFU lower than WT D39 in mock-infected animals and 0.4-2.1 $\log_{10}$ CFU lower in IAV-infected animals ($p<0.01$) (Fig 4A-B, Table S2). By 24 h pbi, titers were statistically similar, yet reduced compared to WT D39 in the lungs (0.5-2.7 $\log_{10}$ CFU reduction; $p>0.05$) and blood (1.3-6.6 $\log_{10}$ CFU reduction; $p>0.05$) of mock-infected animals (Fig 4A, Fig 4C, and Table S2). However, in IAV-infected animals, SGD mutant titers remained significantly lower in the lungs (0.8-2.1 $\log_{10}$ CFU reduction; $p<0.05$) and blood (by 2.2-5.0 $\log_{10}$ CFU reduction; $p<0.01$) at 24 h pbi (Fig 4B, Fig 4D, and Table S2). Despite attenuated growth in the lungs and reduced bacteremia at 24 h pbi, bacterial loads for each SGD mutant remained high in the lungs and blood of coinfected animals at 24 h, 48 h, and 72 h pbi (Fig 4B, Fig 4D, and Table S2).

Similar Viral Load Kinetics

Similar to previous studies (53), viral loads rebounded following coinfection with each SGD mutant bacteria. While viral rebound and clearance occurred with varying dynamics, each was statistically similar to coinfection with WT D39 ($p>0.05$) (Fig 4E, Table S2).

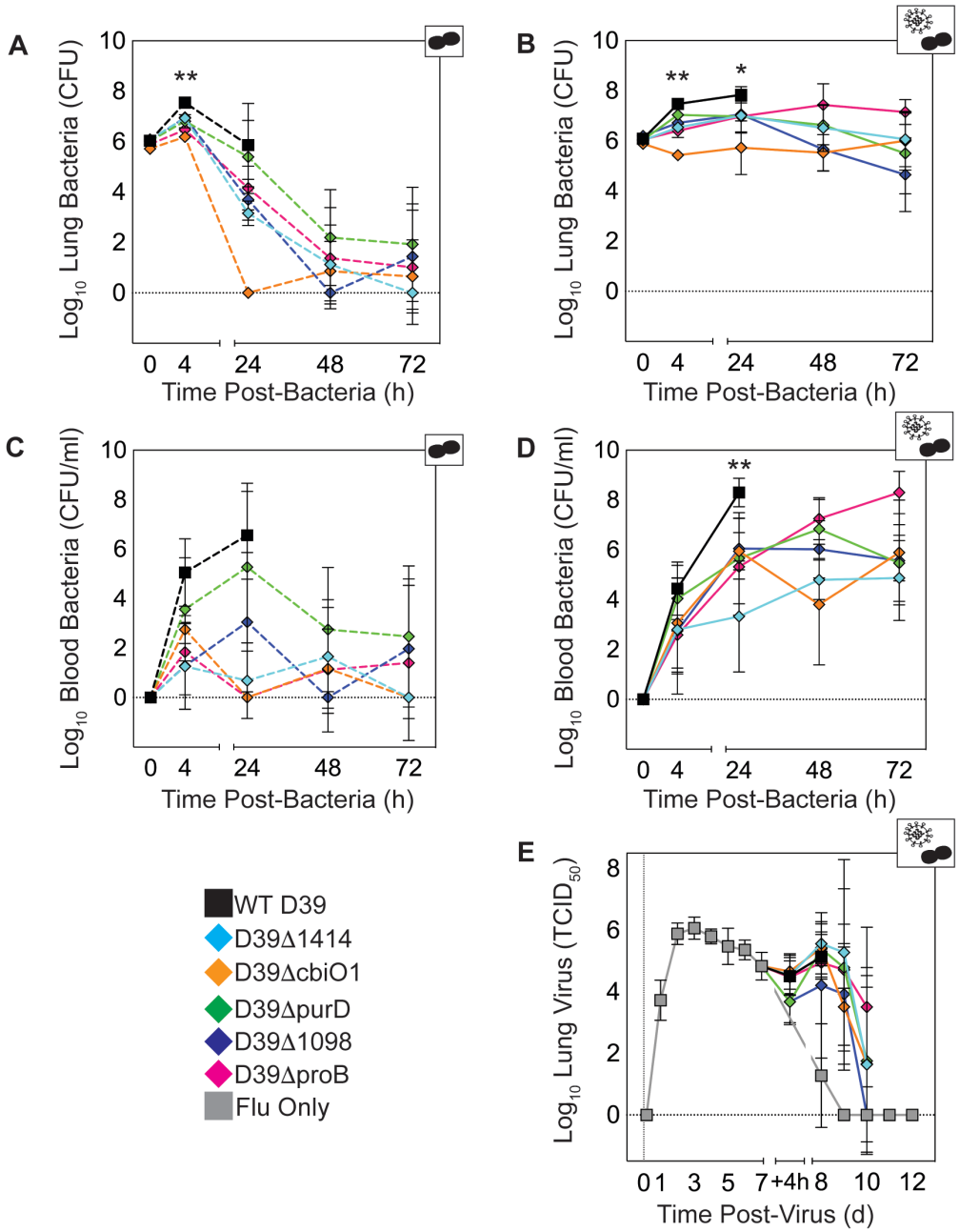

Fig 4: Viral and Bacterial Titer Kinetics. Lung bacterial titers (A-B), blood bacterial titers (C-D), and lung viral titers (E) from groups of mice either mock-infected (PBS) (dashed lines; Panels A, C) or IAV-infected (75 $TCID_{50}$ PR8) (solid lines; Panels B, D, E) followed 7 d later with 10^6 CFU of the indicated bacteria. Signficance is indicated as *p<0.05 and **p<0.01 for each of the SGD mutants compared to WT D39 at the indicated time point.

Data are shown as the mean ± standard deviation (SD) from 5 mice/group. Cartoons indicate infection status of study group (bacteria alone or virus plus bacteria). The $\log_{10}$ change in pathogen loads between each SGD mutant and WT D39, and analysis of variance results are summarized in Table S2**.**

Altered Cytokine and Chemokine Responses

To better understand the reduced morbidity and mortality during infection with the SGD mutants, we examined cytokine and chemokine dynamics in the lungs (Fig 5, Fig S2-S4). In IAV-infected animals, IFN-α, IFN-β, IL-6, KC, MIP-1β and GM-CSF were significantly reduced at 24 h pbi with SGD mutant bacteria compared to WT D39 ($p<0.05$), with the exception of IFN-α during coinfection with D39Δ*1414* ($p=0.95$) and D39Δ*purD* ($p=0.17$) (Fig 5, Fig S2-S4). Interestingly, at 4 h pbi in IAV-infected animals, IFN-α was elevated in D39Δ*1414*, D39Δ*cbiO1*, D39Δ*purD*, and D39Δ*1098* coinfections ($p<0.01$) and IFN-β was elevated in D39Δ*cbiO1* coinfection ($p<0.01$) (Fig 5, Fig S2J and L). In mock-infected animals, IFN-α, IL-6, KC, and MIP-1β were similar at 24 h pbi ($p>0.05$) (Fig 5, Fig S2-S4). IL-1α , IL-1β, MIP-1α, and TNF-α were reduced in both mock- and IAV-infected animals at 24 h pbi with each SGD mutant compared to WT D39 ($p<0.05$), except for D39Δ*purD* in mock-infected animals ($p>0.05$) (Fig 5, Fig S2-S4). Minimal differences were detected for MCP-1, RANTES, IL-2, IFN-γ, IL-10, IL-12(p40), and IL-12(p70), except during primary infection with D39Δ*1098* and D39Δ*proB* (Fig 5, Fig S3-S4).

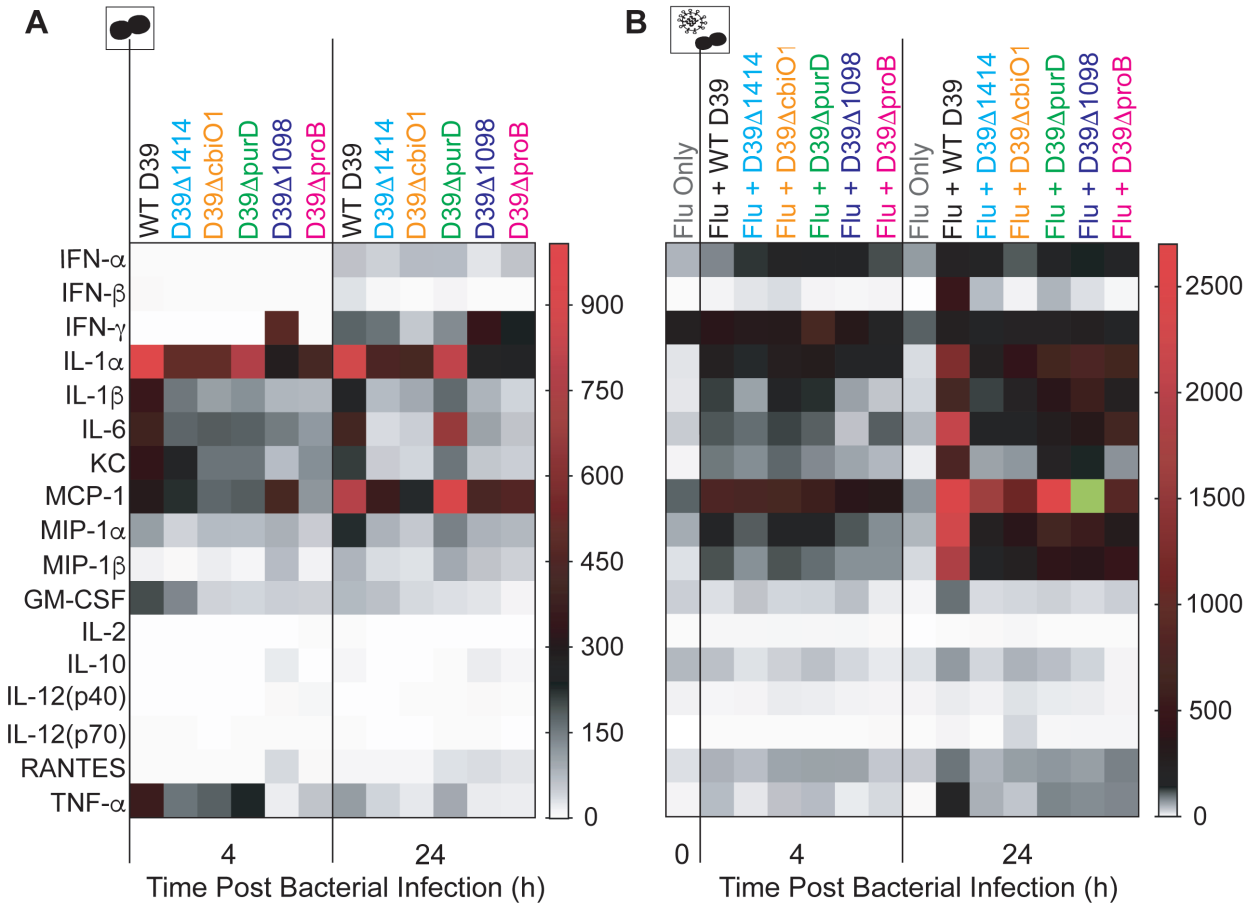

Fig 5: Heat Map of Cytokine and Chemokine Changes. Fold change compared to naïve in the mean value of the indicated cytokine/chemokine at 4 h or 24 h pbi in the lungs of mice mock-infected (PBS) (A) or IAV-infected (75 $TCID_{50}$ PR8) (B) followed 7 d later with 10^6 CFU of the indicated bacteria. The green square is ouside of the listed range and indicates a 4021 fold change. Cartoons indicate infection status of study group (bacteria alone or virus plus bacteria). Plots depicting absolute log_{10} picograms (pg) of measured cytokines and chemokines are in Figs S2-S4.

Reduced Inflamatory Cell Responses

In accordance with the changes detected in pulmonary cytokines and chemokines, infection with SGD mutant bacteria altered the dynamics of select immune cells in the lungs (Fig 6 and Figs S5-S6). In IAV-infected animals, neutrophils (Ly6G^{hi}) were significantly reduced at 4 h pbi with D39Δ*1098* ($p<0.01$) and D39Δ*proB* ($p<0.05$), and at 24 h pbi with D39Δ*1414*, D39Δ*cbiO1*, D39Δ*purD*, and D39Δ*proB* ($p<0.05$) (Fig 6B). Inflammatory macrophages (IMΦs; Ly6G^{-}, CD11c^{hi}, F4/80^{hi}, CD11b^{+}) were also reduced at 4 h pbi during coinfection with D39Δ*1414*, D39Δ*purD*, D39Δ*1098*, and D39Δ*proB* ($p<0.05$) (Fig 6D). D39Δ*cbiO1* did not lead to reduced IMΦs at 4 h pbi ($p=0.14$), but did induce a significant increase in IMΦs at 24 h pbi ($p<0.01$) (Fig 6D). In mock-infected animals, neutrophils and IMΦs were not significantly different at 4 h pbi for any of the SGD mutants ($p>0.05$) (Fig 6A, Fig 6C). At 24 h pbi, neutrophils were reduced by D39Δ*purD* ($p<0.05$) and IMΦs were increased by D39Δ*cbiO1* ($p<0.05$) infection (Fig 6A, Fig 6C). There were minimal differences in T cell populations (Fig S6I-L) or the extent of AMΦ depletion (Ly6G^{-}, CD11c^{hi}, F4/80^{hi}, CD11b^{-}) (Fig 6E-F) in mock- or IAV-infected animals.

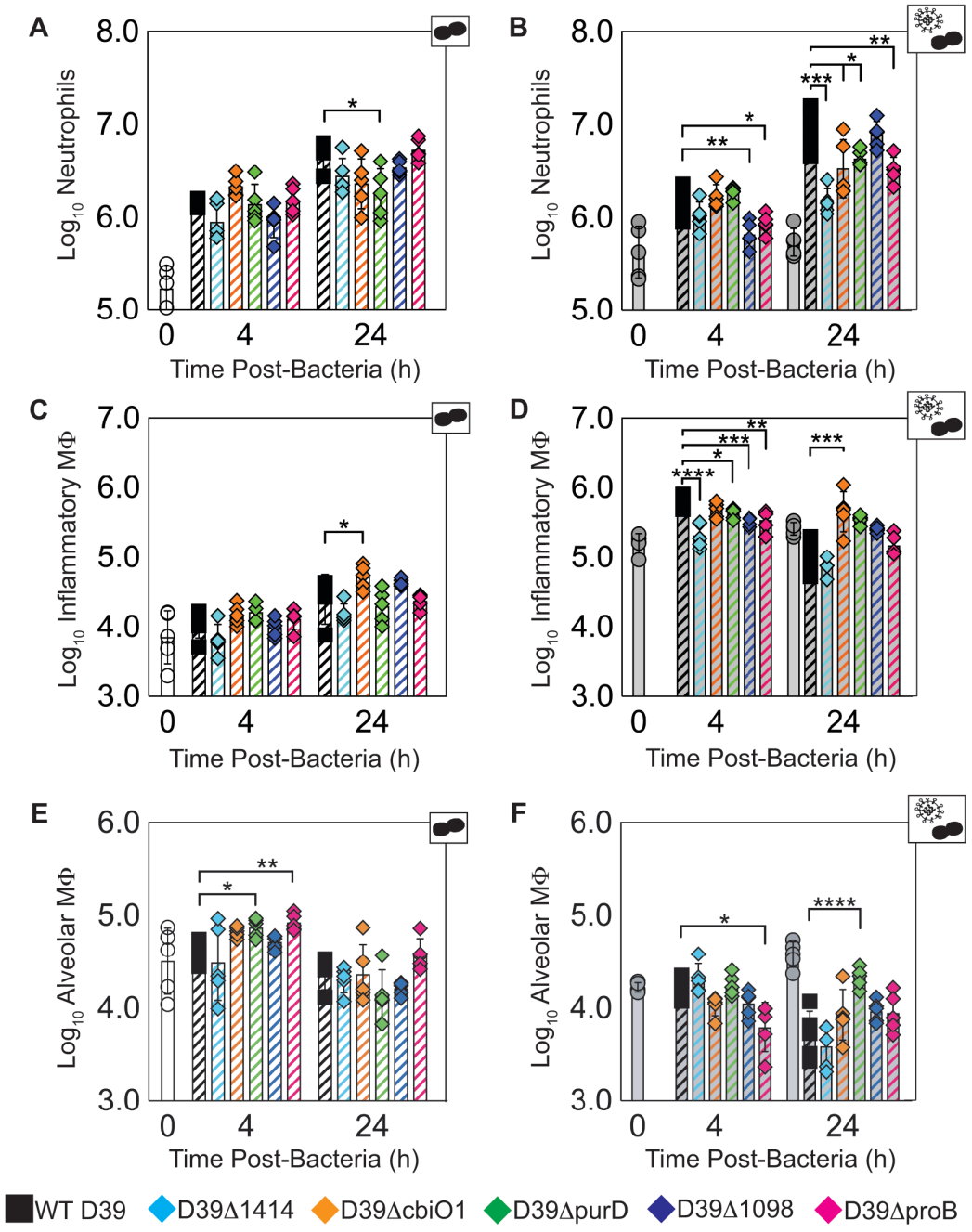

Fig 6: Pulmonary Immune Cell Kinetics. Kinetics at 4 h or 24 h pbi of neutrophils (A-B), inflammatory macrophages (C-D), and alveolar macrophages (E-F) from mice mock-infected (PBS) (Panels A, C, E) or IAV-infected (75 $TCID_{50}$ PR8) (Panels B, D, F) followed 7 d later with 10^6 CFU of the indicated bacteria. Each symbol (circles, squares, or

diamonds) represents a single mouse, and the bars are the geometric mean ± standard deviation (SD)) from 5 mice/group. Mice were either uninfected (open white), IAV-infected only for 7 d (T=0) or 8 d (T=24) (solid grey), bacteria-infected (open hashed, colored), or IAV-bacteria coinfected (solid hashed, colored). Signficance is indicated as *p<0.05, **p<0.01, ***p<0.005, ****p<0.0001. Cartoons indicate infection status of study group (bacteria alone or virus plus bacteria). The flow cytometry gating scheme is in Fig S5 and additional cellular dynamics are in Fig S6.

Reduced Pathology and Altered Neutrophil Phenotype

There was extensive pulmonary consolidation at 24 h pbi in the lungs of mice coinfected with WT D39, as characterized by thickened septa and alveoli filled with a mixture of neutrophils, free bacteria, and proteinaceous exudates (Fig 7A). These lesions were dramatically reduced during coinfection with D39Δ*proB,* D39Δ*1098, and* D39Δ1414 and almost absent in D39Δ*cbiO1* and D39Δ*purD* coinfection (Fig 7A). Immunohistochemical (IHC) staining showed a similar extent of influenza antigen (Fig 7B) but dramatically less bacterial antigen at 24 h pbi during coinfection with each of the SGD mutants (Fig 7C, Fig S7A), which mirrored the pulmonary viral and bacterial loads (Fig 4B, Fig 4E). In WT D39 coinfected animals, intracellular and extracellular bacterial antigen was present throughout influenza-lesioned areas, including pervascular connective tissues, consolidated alveolar parenchyma, and the central hypocellular area of resolving lesions. Bacterial antigen was not detected in the resolving influenza lesions with any of the SGD mutants, except for D39Δ*1098* where few bacteria or pneumococcal antigen-positive macrophages were present. IHC staining also showed massive neutrophil infiltration in

WT D39 coinfection, and the resolving influenza lesions were consistently surrounded by sharply demarcated hypercellular bands composed of mixed viable and degenerating neutrophils (Fig 7C). In contrast, during D39Δ*proB,* D39Δ*purD*, and D39Δ*1098* coinfections, neutrophilic infiltrates generally appeared in clusters within alveoli peripheral to influenza lesions or scattered widely throughout inflamed areas in the lungs. Neutrophil infiltrates in these lungs consisted mostly of intact non-degenerating cells that formed indistinct bands surrounding the influenza lesions (Fig 7C). Animals coinfected with D39Δ*1414* and D39Δ*cbiO1* had the lowest number of neutrophils, which were mostly non-degenerating and scattered throughout inflamed areas (Fig 7C). Neutrophils were rare or absent within the resolving influenza lesions in animals coinfected with an SGD mutant.

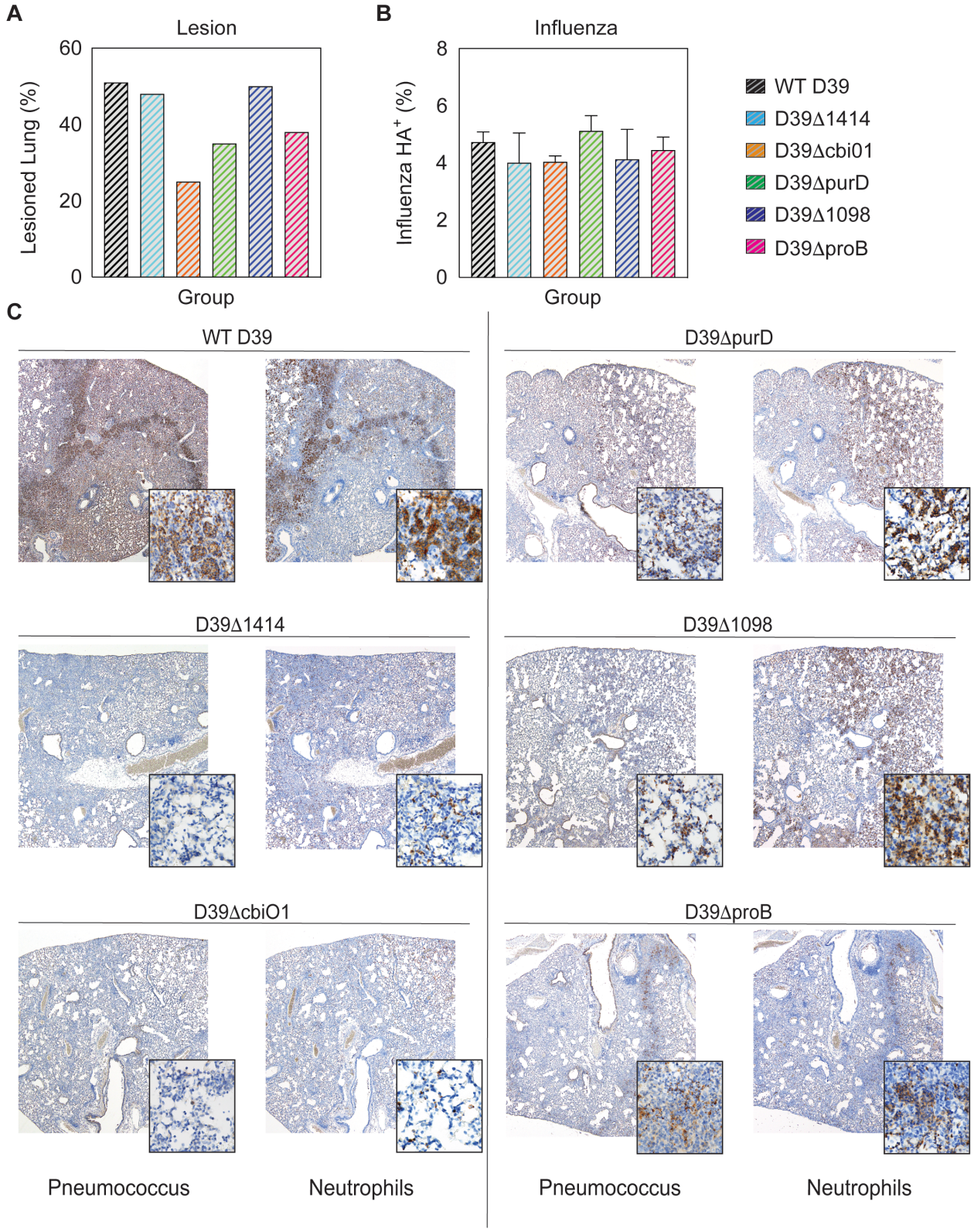
A
Lesion
Lesioned Lung (%)
60
40
20
0
Group
B
Influenza
Influenza HA+ (%)
8
6
4
2
0
Group
WT D39
D39Δ1414
D39Δcbi01
D39ΔpurD
D39Δ1098
D39ΔproB
C
WT D39
D39ΔpurD
D39Δ1414
D39Δ1098
D39ΔcbiO1
D39ΔproB
Pneumococcus
Neutrophils
Pneumococcus
Neutrophils

Fig 7: Lung Pathology During IAV-Pneumococcal Coinfection. Serial sections of lungs at 24 h pbi from mice IAV-infected (75 $TCID_{50}$ PR8) followed 7 d later with 10^6 CFU of the indicated bacteria, stained with hematoxylin and eosin (HE) for histological analysis (Panel A) or immunohistochemistry (IHC) for influenza HA glycoprotein (Panel B), pneumococcus, or neutrophil Ly6G/6C antigen (Panel C). Quantification was performed by a pathologist blinded to the study design (Panel A) or with MIPAR v3.0 image analysis software (Panel B and Figure S7). Representative images are at an original 4x magnification with 60x magnification insets.

Discussion

Pathogenicity during IAV-pneumococcal coinfection is influenced by several pathogen and host factors, including the viral and bacterial strain and doses, and the strength of the inflammatory response (11-16). Our study here highlights the importance of specific genetic factors in contributing to this pathogenicity and to the dysregulated host response. By using Tn-Seq as an unbiased approach, we identified 32 genes as being critical to pneumococcal survival in the IAV-infected host in a time-dependant manner (Table 1, Fig 1). Unsurprisingly, known bacterial virulence genes were not varied in our screen, likely because those factors affect disease equally regardless of viral infection status (40, 41, 43). The identified genes are mostly involved in bacterial metabolism, which supports findings that the lung metabolome is altered during influenza virus infection. Our *in vivo* data suggest that some identified genes function as virulence factors in both mock- and IAV- infected hosts. However, the immunomodulatory effects differed dramatically between heathy mice and those infected with the influenza virus, highlighting the

importance of immune and metabolic alterations in the susceptibility to and severity of bacterial coinfection.

Altered metabolic regulation has been observed during murine influenza virus infection (54-57), *in vitro* influenza virus infection of primary human bronchotracheal epithelial (HBAE) cells (58, 59), and in pediatric patients infected with influenza virus (58). However, even with the knowledge that influenza virus infection induces metabolic changes and that pneumococci modulate metabolic pathways under host-specific pressures (51, 60), the collection of genes identified here was not intuitive nor was their precise contribution to the infection dynamics. It has been shown that purine metabolic pathways are altered in *Haemophilus influenzae* and pneumococci within influenza-infected hosts (49, 50) and in pneumococci within hosts with sickle-cell disease (51). Here, eight genes with roles in purine metabolism were identified, including SPD0058 (*purD*) (61-63) (Table 1, Fig 1). This could indicate a common mechanism for bacterial adaptation within inflammatory environments. In influenza-infected hosts, purine biosynthesis is upregulated (55) and purine analogs can be used to reduce disease severity (e.g., by the antiviral T-705 (64, 65)). However, the intermediates of purine biosynthesis become depleted following bacterial infection (50), rendering genes of de novo purine intermediate synthesis (*purD* and *purC*) critical to coinfecting bacteria (50, 51) (Table 1, Fig 1). Here, it is likely that altered purine scavenging and competition for environmentally available purines/purine intermediates, modulates host immune cell function during infection with D39Δ*purD*, contributing to decreased lethality (Fig 3B) and immunopathology (Fig 7A) in IAV-infected hosts.

Several of the genes identified here act in glutamate/glutamine biosynthesis which, while important for bacterial pathogenesis in otherwise healthy individualts, plays a key role during influenza-pneumococcal coinfection. Here, both genes in the locus pinpointed as the main ABC glutamine/glutamate transporter of pneumococci (SPD1098/1099) (66, 67) were identified in our screen (Table 1, Fig 1). Deleting SPD1098 increased survival by 90% in coinfected animals (Fig 3B), despite neutrophil accumulation equivalent to that in WT D39 coinfection (Fig 6B, Fig 7C). Genes involved in proline biosynthesis, a process downstream of glutamate metabolism (61-63), were also identified, including SPD0822/0823 (*proB/A*) (Table 1, Fig 1). Deletion of SPD0822 (*proB*) delayed mortality during coinfection (Fig 3B) and led to reduced neutrophils and iMΦ in influenza-infected hosts, but not in mock-infected hosts (Fig 6). Glutamine is utilized at a high rate by immune cells and is needed for optimal function of macrophages and neutrophils (68-73). Since pulmonary cells have increased dependence on glutamine during influenza virus infection (57, 58), it is probable that competition for limited, enivonmentally available glutamine altered neutrophil infiltration and function, thereby reducing morbidity and mortality in IAV-infected hosts coinfected with these SGD mutants (Fig 5-7 and Fig 3B). Investigating metabolic alterations of innate immune cells during IAV-infection, would clarify the host-pathogen interactions observed here.

The functions of some genes identified here, including three other ABC transporters (e.g., SPD2047/2048 (*cbiO1/2* and SPD1414), are not well characterized. While it is understood that ABC transporters are important for pneumococcal virulence (35, 36, 74-77),

investigating the impact of each gene identified in our screen provides insight into respiratory changes that occur during influenza virus infection. The role of cobalt in pneumococcal physiology and virulence remains unclear (78, 79), but the cbiO locus (putative cobalt transporter) was previously identified by microarray analysis as necessary for pneumococcal pathogenicity (42). Interestingly, bacteria lacking SPD2047 reach significantly higher lung titers in IAV-infected animals than in mock-infected animals (Fig 4A-D), suggesting that cobalt metabolism may be modified by influenza virus infection. To our knowledge, no study has assessed cobalt dynamics during influenza. The TIGR4 analog of the oxalate/formate antiporter SPD1414 (SP1587) has been shown to be important for bacterial survival in the lungs and blood (36, 80), cerebral spinal fluid (36), and nasopharynx (80). Here, deletion of SPD1414 reduced lethality (Fig 3B), neutrophil infiltration, and pulmonary damage in IAV-infected hosts (Fig 6-7). These results indicate roles for cobalt and oxalate/formate in the susceptibility to pneumococcal pneumonia during influenza-infection.

Mortality during influenza-pneumococcal coinfection is typically associated with an exuberant immune response coupled with high pathogen loads in the lung and the blood (14-16, 24, 81-83). However, reduced inflammation can lessen disease severity even with sustained bacterial loads (26). Here, growth of SGD mutant bacteria in IAV-infected animals was significantly attenuated (0.8-2.1 $\log_{10}$ reduction compared to WT D39), but not strictly correlated to pathogenicity and insufficient to account for the extreme reductions in mortality (up to 90%) (Fig 3B, Fig 4, Table S2) as equivalently reduced bacterial loads of WT D39 in IAV-infected animals still induce significant mortality (FigS8).

In addition, AMΦ, which dictate the initial pneumococcal invasion and growth kinetics during IAV infection (18-20, 23), are not different during coinfection with most SGD mutants compared to WT D39 (Fig 6F). Contraction of the pulmonary $CD8^+$ T cells (84) (Fig S6L) and the rebound of viral loads (Fig 4E) were not altered during coinfection with SGD mutant bacteria, which supports our previous findings that the mechanisms underlying rapid bacterial growth are independent from those that influence the post-bacterial viral rebound and pathogenicity (19, 20). These findings suggest that the observed improvements in immune responses and disease outcome are not solely driven by the differences in bacterial loads. Reduced cytokine levels, specifically lowered type I IFNs (Fig 5, Fig S2J and L) can improve neutrophil function (21, 24, 25, 85-89) and reduce epithelial cell death and lung permeability (90) and, thus, reduce pathogenicity (Fig 3B, Fig 5, and Fig 7). Moreover, reduced neutrophil infiltration and degeneration (Fig 6B, Fig 7C) may have mitigated the damaging cytokine storm that is typically associated with IAV-pneumococcal pneumonia (12-17, 33). A direct correlation between survival and any single host immune response in the early stages of coinfection (0-24 h pbi) was not readily apparent. It is possible that unmeasured components and/or cumulative effects influence lethality at later time points. These studies underscore the independent nature of pathogen growth and pathogenicity and illuminate the difficulty in reducing coinfection pathogenicity to a single variable.

Understanding how bacterial adaptations influence the development of pneumonia during influenza virus infections is important to effectively combat the disease. Here, we provide insight into the contribution of specific pneumococcal genes and to the regulatory host-

pathogen dynamics that arise during IAV-pneumococcal coinfection. Our findings highlight the critical role of influenza-induced metabolic shifts in promoting bacterial infection and altering immune function, and suggest that targeting a single pneumococcal gene or metabolite could be an effective intervention to abrogate bacterial pneumonia during influenza infection. Further dissecting bacterial adaptation may identify additional therapeutic targets that could be used to prevent or treat post-influenza bacterial infections.

Materials and Methods

Ethics Statement All experimental procedures were performed under protocol O2A-020 approved by the Animal Care and Use Committee at St. Jude Children's Research Hospital under relevant institutional and American Veterinary Medical Association (AVMA) guidelines and were performed in a biosafety level 2 facility that is accredited by the American Association for Laboratory Animal Science (AALAS).

Mice Adult (6 week old) female BALB/cJ mice were obtained from Jackson Laboratories (Bar Harbor, ME). Mice were housed in groups of 5 in high-temperature 31.2cm x 23.5cm x 15.2cm polycarbonate cages with isolator lids. Rooms used for housing animals were maintained on a 12:12-hour light:dark cycle at 22 $\pm$ 2°C with 50% humidity in the biosafety level 2 facility at St. Jude Children's Research Hospital (Memphis, TN). Prior to inclusion in the experiments, mice were allowed at least 7 days to acclimate to the animal facility such that they were 7 weeks old at the time of infection. Laboratory Autoclavable Rodent Diet (PMI Nutrition International, St. Louis, MO) and autoclaved water were available ad

libitum. All experiments were performed under an approved protocol and in accordance with the guidelines set forth by the Animal Care and Use Committee at St. Jude Children's Research Hospital.

Tn-Seq Plasmid DNA harboring *magellan6,* a derivative of the Himar1 Mariner transposon, was purified from *E. coli* with the Qiagen mini plasmid preparation kit (Qiagen). Pneumococcal DNA was isolated by phenol/chloroform extraction and ethanol precipitation from an exponentially growing culture in ThyB media (30 mg/ml Todd-Hewitt Broth powder and 0.2 mg/ml yeast). *In vitro, magellan6* transposition reactions were carried out with purified MarC9 transposase, 1 µg of pneumococcal target DNA and 1 µg of *magellan6* plasmid DNA. Reactions were incubated for 1 h at 30°C, inactivated for 20 min at 72°C, ethanol precipitated and resuspended in gap repair buffer [50 mM Tris (pH 7.8), 10 mM $MgCl_2$, 1 mM DTT, 100 nM dNTPs and 50 ng BSA]. Repair of transposition product gaps was performed with *E. coli* DNA ligase overnight at 16°C. Repaired transposition products were transformed into naturally competent pneumococcal strain D39. The following day, colonies were scraped off tryptic soy-agar (TSA) plates supplemented with 3% sheep erythrocytes and 200 mg/ml spectinomycin (TSA-Spec), pooled into libraries of approximately 50,000 transformants/library, split up into multiple starter cultures and stored at -20°C.

Bacterial Fitness By Tn-Seq Bacteria were collected from the blood and lungs of each infected mouse at 12 h pbi or 24 h pbi and plated on TSA-Spec plates as indicated (Lung and Blood Harvesting). Later time points could not be examined due to insufficient

numbers of surviving mice. Bacteria were incubated for 12 h at 37°C then collected in ThyB media and centrifuged at 4°C, 500xg for 10 min. The media supernatant was removed and the pellets were stored at -20°C. Gene identification by Tn-Seq was performed as described previously (51, 52, 80). The samples at each of the three time points (pre-selection (inoculum, t_1) and post-selection (after infection, 12 h (t_2) or 24 h (t_3) pbi), were sequenced in rapid run mode on an Illumina HiSeq 2000 using the primers and cycle conditions in Table S1. For each insertion, the fitness *Wi*, was calculated by comparing the fold expansion of the mutant relative to the rest of the population with the following equation (91),

$$W_i = \frac{\ln\ [N_i(t_{2,3})d/N_i(t_1)]}{\ln\ [(1 - N_i(t_{2,3}))d/(1 - N_i(t_{2,3}))]}$$

where the mutant frequency at time 0 and harvest are $N_i(t_1)$ and $N_i(t_{2,3})$, respectively. The expansion factor (d) accounts for bacterial growth during library selection. Additional details of the method are included in the Supplementary Information.

Infectious Agents All experiments were done using the mouse adapted influenza A/Puerto Rico/8/34 (H1N1) (PR8) and type 2 pneumococcal strain D39 variants. Transposon mutant library used for infections was generated as described above (Tn-Seq). To generate the single-gene deletion (SGD) mutants, genomic DNA was isolated from WT D39 as above (Tn-Seq) and used as the template for gene SOEing PCR (92, 93). In brief, regions flanking the D39 locus targeted for deletion and containing overhangs complementary to the erythromycin (ERM) resistance cassette (*ermB*) (labeled regions A and B) were generated using the primer sets and cycle conditions

indicated in Table S1B (EasyA PCR kit (Agilent Tech) and BioRad T100 thermal cycler). Products were purified using the Zymoclean gel DNA recovery kit (Zymo Research), recombined by PCR (TaKaRa PCR kit (Clontech Laboratories)) using the primers and cycle conditions in Table S1C, and transformed into D39. Transformed bacteria were selected after overnight growth on TSA plates containing 1 µg/ml ERM (TSA-ERM). Infection stocks were grown in ThyB media containing 1 µg/ml ERM, and stored at -80°C in 12% glycerol. ERM resistance cassette insertion and target locus deletion were confirmed by PCR with the primer sets in Table S1D.

Infection Experiments The viral infectious dose ($TCID_{50}$) was determined by interpolation using the method of Reed and Muench (94) using serial dilutions of virus on Madin-Darby canine kidney (MDCK) cells. Bacterial infectious doses (CFU) were determined by serial dilutions on TSA (WT), TSA-ERM (SGD mutants), or TSA-Spec (Tn-seq) plates. Frozen stocks of inocula were diluted in sterile PBS and administered intranasally to groups of 5 (for kinetics) or 10 (for bacteria collection and survival) mice lightly anesthetized with 2.5% inhaled isoflurane (Baxter, Deerfield, IL) in a total volume of 100 µl (50 µl per nostril). Mice were inoculated with either PBS or 75 $TCID_{50}$ PR8 at day 0 then with 10^6 CFU of the transposon mutant library, D39, or indicated SGD mutant (in 100 µl), 7 days later. This dose of bacteria was chosen to ensure sufficient amounts of bacteria were recovered in Tn-Seq experiments and the CFU of each inoculum was confirmed as above. For bacterial sequencing, 500 µl of the inoculum was plated on TSA-Spec plates (100 µl/plate) (t_1 in Bacterial Fitness By Tn-Seq). Animals were weighed at

the onset of infection and each subsequent day to monitor illness and mortality. Mice were euthanized if they became moribund or lost 30% of their starting body weight.

Lung and Blood Harvesting Mice were euthanized by CO_2 asphyxiation. For bacterial sequencing, lungs were perfused with 10 ml PBS, aseptically harvested, washed three times in PBS, and placed on ice in 500 µl PBS. The post-perfusion fluid (mixture of blood and PBS) was plated immediately on TSA-Spec plates (150 µl/plate). Lungs were then enzyme digested with collagenase (1 mg/ml, Sigma), and physically homogenized by syringe plunger against a 40µm cell strainer. Cell suspensions were centrifuged at 4°C, 500xg for 7 min and the supernatant was plated on TSA-spec plates (500 µl; 100 µl/plate). For *in vitro* SGD growth, lungs were homogenized (Omni TH-01 with 5mm flat blade) and centrifuged at 4°C, 500xg for 7 min. For *in vivo* kinetics, unperfused lungs were enzyme digested with collagenase as above and supernatants were used to quantify viral titers, bacterial titers, cytokine/chemokine levels (5 mice/group). Following red blood cell lysis, cells were washed in MACS buffer (PBS, 0.1 M EDTA, 0.01 M HEPES, 5 mM EDTA and 5% heat-inactivated FBS), counted with trypan blue exclusion using a Cell Countess System (Invitrogen, Grand Island, NY), and prepared for flow cytometric analysis as described below.

***In vitro* Kinetics** Bacteria were grown at 37ºC in 1.0 ml of ThyB media, PBS, or lung homogenate supernatants (s/n). At each time point, 50 µl was removed, serially diluted in PBS, and plated on TSA (WT) or TSA-ERM plates. Bacterial titers were normalized to the total volume. 3 biological replicates were performed.

Lung and Blood Titers For each mouse, viral titers were obtained using serial dilutions on MDCK monolayers, and bacterial titers were obtained using serial dilutions on TSA (WT) or TSA-ERM (SGD mutants) plates.

Cytokines Cytokines and chemokines were measured in lung supernatant by luminex (GM-CSF, IFN-γ, IL-1α, IL-1β, IL-2, IL-6, IL-10, IL-12(p40), IL-12(p70), KC, MCP-1, MIP-1α, MIP-1β, RANTES, and TNF-α) and ELISA (IFN-α,β). Prior to use, cell debris and aggregates were removed by centrifugation at 4°C, 400xg. Milliplex magnetic bead cytokine/chemokine plates (Millipore) were prepared according to manufacturer's instructions. Analysis was done using a BioRad BioPlex (HTF System) and Luminex xPonent software. ELISAs for IFN-α and IFN-β (PBL Assay Science) were prepared according to the manufacturer's instructions. Plates were read at 450 nm and analyzed using elisaanalysis.com. Mean concentrations of duplicate samples were calculated by construction of standard curves using a weighted 5PL and 4PL regression for the Milliplex and ELISA data, respectively. Absolute quantities of each cytokine/chemokine were calculated based on mean concentration of replicate samples normalized to the lung supernatant volume collected during tissue processing.

Flow Cytometric Analysis Flow cytometry (LSRII Fortessa; Becton Dickinson, San Jose, CA) was performed on single cell suspensions after incubation with 200 μl of 1:2 dilution of Fc block (human-γ globulin) on ice for 30 min, followed by surface marker staining with anti-mouse antibodies: CD11c (clone N418, eFluor450, eBioscience),

CD11b (clone M1/70, Alexa700, BD Biosciences), Ly6G (clone 1A8, PerCp-Cy5.5, Biolegend), Ly6C (clone HK1.4, APC, eBioscience), F4/80 (clone BM8, PE, eBioscience), CD3e (clone 145-2C11, PE-Cy7, BD Biosciences or BV785, Biolegend), CD4 (clone RM4-5, PE-Cy5, BD Biosciences), CD8α (clone 53-6.7, BV605, BD Biosciences), CD49b (clone DX5, APC-Cy7, Biolegend or APC-e780, Affymetrix Inc) and MHC-II (clone M5/114.15.2, FITC, eBioscience). The data were analyzed using FlowJo 10.4.2 (Tree Star, Ashland, OR) where viable cells were gated from a forward scatter/side scatter plot and singlet inclusion. Following neutrophil exclusion (Ly6G^{hi}), macrophages (MΦ) were gated as CD11c^{hi}F4/80^{hi} with alveolar macrophages (AMΦ) sub-gated as CD11b^{-} and inflammatory macrophages (iMΦ) as CD11b^{+}. After macrophage exclusion, T cell populations were gated as CD3e^{+} and subgated into CD8 T cells (CD3^{+}CD8^{+}CD4^{-}DX5^{-}) and CD4 T cells (CD3^{+}CD8^{-}CD4^{+}DX5^{-}). From the CD3e^{-} population, natural killer (NK) cells were gated as CD3^{-}DX5^{+} and dendritic cells (DCs) as CD3^{-}DX5^{-}. DC were further gated into three subsets of DC; CD11c^{+}CD11b^{-}, CD11c^{+}CD11b^{+}, and CD11c^{-}CD11b^{+} (Fig S5). The expression levels of MHC-II was used to confirm the identities and activation of MΦ and DC subsets. The absolute numbers of cell types were calculated based on viable events analyzed by flow cytometry and normalized to the total number of viable cells per sample.

Histology Mice were euthanized by CO_2 asphyxiation and lungs were inflated *in situ* via tracheal infusion with 10% neutral-buffered formalin solution (NBF; ThermoFisher Scientific, Waltham, MA), followed by continued fixation in NBF for at least 2 weeks before being embedded in paraffin, sectioned at 4 μm, mounted on positively charged glass

slides (Superfrost Plus; Thermo Fisher Scientific, Waltham, MA), and dried at 60°C for 20 min. Tissue sections were stained with hematoxylin and eosin (HE) or subjected to immunohistochemical (IHC) staining to detect influenza antigen, pneumococcus, and neutrophils. For detection of these targets, tissue sections underwent antigen retrieval in a prediluted Cell Conditioning Solution (CC1; Cat# 950-124; Ventana Medical Systems, Indianapolis, IN) for 32 min on a Discovery Ultra immunostainer (Ventana Medical Systems, Tucson, AZ). Primary antibodies included (i) a polyclonal goat antibody raised against the HA glycoprotein of B/Florida/04/2006 (Yamagata lineage) influenza virus diluted 1:2000 (cat# I7650-05G, US Biologicals, Swampscott, MA), (ii) a rabbit polyclonal antibody to *Streptococcus pneumoniae* diluted 1:1000 (cat# NB100-64502; Novus Biologicals, Littleton, CO), and (iii) a rat monoclonal antibody to neutrophils (Ly6G6C) diluted 1:50 (cat# NB600-1387; Novus Biologicals, Littleton, CO). Binding was detected using OmniMap anti-Goat (#760-4647), anti-Rabbit (#760-4311), and anti-Rat (#760-4457) HRP (RUO) respectively (Ventana Medical Systems), with DISCOVERY ChromoMap DAB Kit (Ventana Medical Systems) as chromogenic substrate. Stained sections were examined by a pathologist (PV) blinded to the experimental group assignments. IHC was quantified (APS) using the provided immunohistochemistry recipe #L006-02 in MIPAR v3.0.

Statistical Analysis Significant differences in Kaplan-Meier survival curves were calculated using the log rank test. *In vitro* growth/decay rates were analyzed by nonlinear regression of $\log_{10}$ values, and linear slopes were compared by analysis of covariance (ANCOVA). The remainder of statistical analyses were performed on linear values.

Unpaired t-tests were done to analyze *in vitro* growth dynamics in ThyB and lung cultures. Analyses of variance (ANOVA) were performed using a Dunnett correction for multiple comparisons (to WT D39) to analyze *in vivo* differences including, lung and blood bacterial loads, viral loads, immune cells, cytokines, and chemokines (GraphPad Prism 7.0c). The confidence interval of significance was set to 95%, and p values less than 0.05 were considered significant.

Contributions

AMS, JAM, and JR conceived the experiments. AMS, AI, CB, and MJ generated the mutant libraries. DR, RC, and TvO completed the sequence analyses. APS and LL generated SGD mutant bacteria. AMS, APS, LL, and MJ performed *in vitro/in vivo* experiments. AMS, APS, LL, and GH performed the data analysis. PV performed the histological analysis. AMS and APS wrote the manuscript.

Acknowledgements

This work was supported by NIH grant AI100946, AI125324, and AI139088 (AMS), PATRIC DBP (AMS, JR, JAM), ALSAC (APS, LCL, SW, RC, AI, CB, PV, DR, MDLJ, JAM, JR), NIH grant R25CA23944 (GH), and NIH grants R01AI110724, U01AI124302, and R21AI117247 (TvO).

References

1. Morens David M, Taubenberger Jeffery K, Fauci Anthony S. 2008. Predominant Role of Bacterial Pneumonia as a Cause of Death in Pandemic Influenza: Implications for Pandemic Influenza Preparedness. The Journal of Infectious Diseases 198:962-970.
2. Gill JR, Sheng Z-M, Ely SF, Guinee DG, Beasley MB, Suh J, Deshpande C, Mollura DJ, Morens DM, Bray M, Travis WD, Taubenberger JK. 2010. Pulmonary pathologic findings of fatal 2009 pandemic influenza A/H1N1 viral infections. Archives of Pathology & Laboratory Medicine 134:235-243.
3. Weinberger DM, Simonsen L, Jordan R, Steiner C, Miller M, Viboud C. 2012. Impact of the 2009 Influenza Pandemic on Pneumococcal Pneumonia Hospitalizations in the United States. The Journal of Infectious Diseases 205:458-465.
4. Louria DB, Blumenfeld HL, Ellis JT, Kilbourne ED, Rogers DE. 1959. STUDIES ON INFLUENZA IN THE PANDEMIC OF 1957-1958. II. PULMONARY COMPLICATIONS OF INFLUENZA*†. Journal of Clinical Investigation 38:213-265.
5. Brundage JF, Shanks GD. 2008. Deaths from Bacterial Pneumonia during 1918–19 Influenza Pandemic. Emerging Infectious Diseases 14:1193-1199.
6. Klugman KP, Chien Y-W, Madhi SA. 2009. Pneumococcal pneumonia and influenza: A deadly combination. Vaccine 27:C9-C14.

23 7. Morens DM, Taubenberger JK, Fauci AS. 2009. The Persistent Legacy of the 1918
24 Influenza Virus. New England Journal of Medicine 361:225-229.
25 8. Gillet Y, Vanhems P, Lina G, Bes M, Vandenesch F, Floret D, Etienne J. 2007.
26 Factors Predicting Mortality in Necrotizing Community-Acquired Pneumonia
27 Caused by Staphylococcus aureus Containing Panton-Valentine Leukocidin.
28 Clinical Infectious Diseases 45:315-321.
29 9. Iverson AR, Boyd KL, McAuley JL, Plano LR, Hart ME, McCullers JA. 2011.
30 Influenza virus primes mice for pneumonia from Staphylococcus aureus. The
31 Journal of Infectious Diseases 203:880-888.
32 10. McCullers Jonathan A, McAuley Julie L, Browall S, Iverson Amy R, Boyd Kelli L,
33 Henriques Normark B. 2010. Influenza Enhances Susceptibility to Natural
34 Acquisition of and Disease due to Streptococcus pneumoniae in Ferrets.
35 The Journal of Infectious Diseases 202:1287-1295.
36 11. Smith AM, McCullers JA. 2014. Secondary Bacterial Infections in Influenza Virus
37 Infection Pathogenesis, p 327-356. *In* Compans RW, Oldstone MBA (ed),
38 Influenza Pathogenesis and Control - Volume I, vol 385. Springer International
39 Publishing, Cham.
40 12. McCullers JA. 2014. The co-pathogenesis of influenza viruses with bacteria in the
41 lung. Nature Reviews Microbiology 12:252-262.
42 13. Short KR, Habets MN, Hermans PWM, Diavatopoulos DA. 2012. Interactions
43 between Streptococcus pneumoniae and influenza virus: a mutually
44 beneficial relationship? Future Microbiology 7:609-624.

45 14. Rynda-Apple A, Robinson KM, Alcorn JF. 2015. Influenza and Bacterial
46 Superinfection: Illuminating the Immunologic Mechanisms of Disease. Infection
47 and Immunity 83:3764-3770.
48 15. Metzger DW, Sun K. 2013. Immune Dysfunction and Bacterial Coinfections
49 following Influenza. The Journal of Immunology 191:2047-2052.
50 16. Robinson KM, Kolls JK, Alcorn JF. 2015. The immunology of influenza virus-
51 associated bacterial pneumonia. Current Opinion in Immunology 34:59-67.
52 17. Kash JC, Taubenberger JK. 2015. The Role of Viral, Host, and Secondary
53 Bacterial Factors in Influenza Pathogenesis. The American Journal of Pathology
54 185:1528-1536.
55 18. Ghoneim HE, Thomas PG, McCullers JA. 2013. Depletion of Alveolar
56 Macrophages during Influenza Infection Facilitates Bacterial Superinfections. The
57 Journal of Immunology 191:1250-1259.
58 19. Smith AM, Adler FR, Ribeiro RM, Gutenkunst RN, McAuley JL, McCullers JA,
59 Perelson AS. 2013. Kinetics of Coinfection with Influenza A Virus and
60 Streptococcus pneumoniae. PLoS Pathogens 9:e1003238.
61 20. Smith AM, Smith AP. 2016. A Critical, Nonlinear Threshold Dictates Bacterial
62 Invasion and Initial Kinetics During Influenza. Scientific Reports 6.
63 21. Sun K, Metzger DW. 2008. Inhibition of pulmonary antibacterial defense by
64 interferon-γ during recovery from influenza infection. Nature Medicine 14:558-564.
65 22. Janssen WJ, Barthel L, Muldrow A, Oberley-Deegan RE, Kearns MT, Jakubzick
66 C, Henson PM. 2011. Fas determines differential fates of resident and recruited

67 macrophages during resolution of acute lung injury. Am J Respir Crit Care Med
68 184:547-60.
69 23. Califano D, Furuya Y, Metzger DW. 2018. Effects of Influenza on Alveolar
70 Macrophage Viability Are Dependent on Mouse Genetic Strain. Journal of
71 Immunology (Baltimore, Md: 1950) 201:134-144.
72 24. Shahangian A, Chow EK, Tian X, Kang JR, Ghaffari A, Liu SY, Belperio JA, Cheng
73 G, Deng JC. 2009. Type I IFNs mediate development of postinfluenza bacterial
74 pneumonia in mice. Journal of Clinical Investigation 119:1910-1920.
75 25. Tian X, Xu F, Lung WY, Meyerson C, Ghaffari AA, Cheng G, Deng JC. 2012. Poly
76 I:C Enhances Susceptibility to Secondary Pulmonary Infections by Gram-Positive
77 Bacteria. PLoS ONE 7:e41879.
78 26. Karlström Å, Heston SM, Boyd KL, Tuomanen EI, McCullers JA. 2011. Toll-Like
79 Receptor 2 Mediates Fatal Immunopathology in Mice During Treatment of
80 Secondary Pneumococcal Pneumonia Following Influenza. The Journal of
81 Infectious Diseases 204:1358-1366.
82 27. McNamee LA, Harmsen AG. 2006. Both Influenza-Induced Neutrophil Dysfunction
83 and Neutrophil-Independent Mechanisms Contribute to Increased Susceptibility to
84 a Secondary Streptococcus pneumoniae Infection. Infection and Immunity
85 74:6707-6721.
86 28. LeVine AM, Koeningsknecht V, Stark JM. 2001. Decreased pulmonary clearance
87 of S. pneumoniae following influenza A infection in mice. Journal of Virological
88 Methods 94:173-186.

89 29. Sun K, Metzger DW. 2014. Influenza Infection Suppresses NADPH Oxidase-
90 Dependent Phagocytic Bacterial Clearance and Enhances Susceptibility to
91 Secondary Methicillin-Resistant Staphylococcus aureus Infection. The Journal of
92 Immunology 192:3301-3307.
93 30. Abramson JS, Mills EL, Giebink GS, Quie PG. 1982. Depression of monocyte and
94 polymorphonuclear leukocyte oxidative metabolism and bactericidal capacity by
95 influenza A virus. Infection and Immunity 35:350-355.
96 31. Abramson JS, Lewis JC, Lyles DS, Heller KA, Mills EL, Bass DA. 1982. Inhibition
97 of neutrophil lysosome-phagosome fusion associated with influenza virus infection
98 in vitro. Role in depressed bactericidal activity. The Journal of Clinical Investigation
99 69:1393-1397.
100 32. Bansal S, Yajjala VK, Bauer C, Sun K. 2018. IL-1 Signaling Prevents Alveolar
101 Macrophage Depletion during Influenza and Streptococcus pneumoniae
102 Coinfection. J Immunol 200:1425-1433.
103 33. Rudd JM, Ashar HK, Chow VT, Teluguakula N. 2016. Lethal Synergism between
104 Influenza and Streptococcus pneumoniae. J Infect Pulm Dis 2.
105 34. Rowe HM, Karlsson E, Echlin H, Chang TC, Wang L, van Opijnen T, Pounds SB,
106 Schultz-Cherry S, Rosch JW. 2019. Bacterial Factors Required for Transmission
107 of Streptococcus pneumoniae in Mammalian Hosts. Cell Host Microbe 25:884-891
108 e6.
109 35. Tettelin H. 2001. Complete Genome Sequence of a Virulent Isolate of
110 Streptococcus pneumoniae. Science 293:498-506.

111 36. Orihuela CJ, Radin JN, Sublett JE, Gao G, Kaushal D, Tuomanen EI. 2004.
112 Microarray analysis of pneumococcal gene expression during invasive disease.
113 Infect Immun 72:5582-96.
114 37. Ogunniyi AD, Giammarinaro P, Paton JC. 2002. The genes encoding virulence-
115 associated proteins and the capsule of Streptococcus pneumoniae are
116 upregulated and differentially expressed in vivo. Microbiology (Reading, England)
117 148:2045-2053.
118 38. LeMessurier KS, Ogunniyi AD, Paton JC. 2006. Differential expression of key
119 pneumococcal virulence genes in vivo. Microbiology (Reading, England) 152:305-
120 311.
121 39. Mahdi LK, Ogunniyi AD, LeMessurier KS, Paton JC. 2008. Pneumococcal
122 virulence gene expression and host cytokine profiles during pathogenesis of
123 invasive disease. Infection and Immunity 76:646-657.
124 40. Kadioglu A, Weiser JN, Paton JC, Andrew PW. 2008. The role of Streptococcus
125 pneumoniae virulence factors in host respiratory colonization and disease. Nat Rev
126 Microbiol 6:288-301.
127 41. Mitchell AM, Mitchell TJ. 2010. Streptococcus pneumoniae: virulence factors and
128 variation. Clinical Microbiology and Infection 16:411-418.
129 42. Ogunniyi AD, Mahdi LK, Trappetti C, Verhoeven N, Mermans D, Van der Hoek
130 MB, Plumptre CD, Paton JC. 2012. Identification of genes that contribute to the
131 pathogenesis of invasive pneumococcal disease by in vivo transcriptomic analysis.
132 Infection and Immunity 80:3268-3278.

133 43. Henriques-Normark B, Tuomanen EI. 2013. The pneumococcus: epidemiology,
134 microbiology, and pathogenesis. Cold Spring Harb Perspect Med 3.
135 44. Molzen TE, Burghout P, Bootsma HJ, Brandt CT, van der Gaast-de Jongh CE,
136 Eleveld MJ, Verbeek MM, Frimodt-Moller N, Ostergaard C, Hermans PW. 2011.
137 Genome-wide identification of Streptococcus pneumoniae genes essential for
138 bacterial replication during experimental meningitis. Infect Immun 79:288-97.
139 45. D'Mello A, Riegler AN, Martinez E, Beno SM, Ricketts TD, Foxman EF, Orihuela
140 CJ, Tettelin H. 2020. An in vivo atlas of host-pathogen transcriptomes during
141 Streptococcus pneumoniae colonization and disease. Proc Natl Acad Sci U S A
142 117:33507-33518.
143 46. Siegel Steven J, Roche Aoife M, Weiser Jeffrey N. 2014. Influenza Promotes
144 Pneumococcal Growth during Coinfection by Providing Host Sialylated Substrates
145 as a Nutrient Source. Cell Host & Microbe 16:55-67.
146 47. Peltola Ville T, Murti KG, McCullers Jonathan A. 2005. Influenza Virus
147 Neuraminidase Contributes to Secondary Bacterial Pneumonia. The Journal of
148 Infectious Diseases 192:249-257.
149 48. McCullers Jonathan A, Bartmess Kimberly C. 2003. Role of Neuraminidase in
150 Lethal Synergism between Influenza Virus and Streptococcus pneumoniae.
151 The Journal of Infectious Diseases 187:1000-1009.
152 49. Liu X, Kimmey JM, Matarazzo L, de Bakker V, Van Maele L, Sirard JC, Nizet V,
153 Veening JW. 2020. Exploration of Bacterial Bottlenecks and Streptococcus
154 pneumoniae Pathogenesis by CRISPRi-Seq. Cell Host Microbe
155 doi:10.1016/j.chom.2020.10.001.

156 50. Wong SM, Bernui M, Shen H, Akerley BJ. 2013. Genome-wide fitness profiling
157 reveals adaptations required by Haemophilus in coinfection with influenza A virus
158 in the murine lung. Proceedings of the National Academy of Sciences 110:15413-
159 15418.
160 51. Carter R, Wolf J, van Opijnen T, Muller M, Obert C, Burnham C, Mann B, Li Y,
161 Hayden Randall T, Pestina T, Persons D, Camilli A, Flynn Patricia M, Tuomanen
162 Elaine I, Rosch Jason W. 2014. Genomic Analyses of Pneumococci from Children
163 with Sickle Cell Disease Expose Host-Specific Bacterial Adaptations and Deficits
164 in Current Interventions. Cell Host & Microbe 15:587-599.
165 52. van Opijnen T, Bodi KL, Camilli A. 2009. Tn-seq: high-throughput parallel
166 sequencing for fitness and genetic interaction studies in microorganisms. Nature
167 Methods 6:767-772.
168 53. Smith AM. 2018. Host-pathogen kinetics during influenza infection and coinfection:
169 insights from predictive modeling. Immunol Rev 285:97-112.
170 54. Milner JJ, Wang J, Sheridan PA, Ebbels T, Beck MA, Saric J. 2014. 1H NMR-
171 based profiling reveals differential immune-metabolic networks during influenza
172 virus infection in obese mice. PLoS One 9:e97238.
173 55. Chandler JD, Hu X, Ko E-J, Park S, Lee Y-T, Orr M, Fernandes J, Uppal K, Kang
174 S-M, Jones DP, Go Y-M. 2016. Metabolic pathways of lung inflammation revealed
175 by high-resolution metabolomics (HRM) of H1N1 influenza virus infection in mice.
176 American Journal of Physiology-Regulatory, Integrative and Comparative
177 Physiology 311:R906-R916.

178 56. Cui L, Zheng D, Lee YH, Chan TK, Kumar Y, Ho WE, Chen JZ, Tannenbaum SR,
179 Ong CN. 2016. Metabolomics Investigation Reveals Metabolite Mediators
180 Associated with Acute Lung Injury and Repair in a Murine Model of Influenza
181 Pneumonia. Scientific Reports 6.
182 57. Rezinciuc S, Bezavada L, Bahadoran A, Duan S, Wang R, Lopez-Ferrer D, Zink
183 EE, Finklestein D, Green DR, Pasa-Tolic L, Thomas PG, Smallwood HS. 2020.
184 Dynamic metabolic reprogramming in dendritic cells: an early response to
185 influenza infection that is essential for effector function. bioRxiv
186 doi:10.1101/2020.01.14.906826:2020.01.14.906826.
187 58. Smallwood HS, Duan S, Morfouace M, Rezinciuc S, Shulkin BL, Shelat A, Zink
188 EE, Milasta S, Bajracharya R, Oluwaseum AJ, Roussel MF, Green DR, Pasa-Tolic
189 L, Thomas PG. 2017. Targeting Metabolic Reprogramming by Influenza Infection
190 for Therapeutic Intervention. Cell Reports 19:1640-1653.
191 59. Kroeker AL, Ezzati P, Coombs KM, Halayko AJ. 2013. Influenza A Infection of
192 Primary Human Airway Epithelial Cells Up-Regulates Proteins Related to Purine
193 Metabolism and Ubiquitin-Related Signaling. Journal of Proteome Research
194 12:3139-3151.
195 60. Syk A, Norman M, Fernebro J, Gallotta M, Farmand S, Sandgren A, Normark S,
196 Henriques-Normark B. 2014. Emergence of hypervirulent mutants resistant to
197 early clearance during systemic serotype 1 pneumococcal infection in mice and
198 humans. J Infect Dis 210:4-13.

199 61. Kanehisa M, Furumichi M, Tanabe M, Sato Y, Morishima K. 2017. KEGG: new
200 perspectives on genomes, pathways, diseases and drugs. Nucleic Acids Res
201 45:D353-D361.
202 62. Kanehisa M, Goto S. 2000. KEGG: kyoto encyclopedia of genes and genomes.
203 Nucleic Acids Res 28:27-30.
204 63. Kanehisa M, Sato Y, Kawashima M, Furumichi M, Tanabe M. 2016. KEGG as a
205 reference resource for gene and protein annotation. Nucleic Acids Res 44:D457-
206 62.
207 64. Furuta Y, Takahashi K, Kuno-Maekawa M, Sangawa H, Uehara S, Kozaki K,
208 Nomura N, Egawa H, Shiraki K. 2005. Mechanism of Action of T-705 against
209 Influenza Virus. Antimicrobial Agents and Chemotherapy 49:981-986.
210 65. Kiso M, Takahashi K, Sakai-Tagawa Y, Shinya K, Sakabe S, Le QM, Ozawa M,
211 Furuta Y, Kawaoka Y. 2010. T-705 (favipiravir) activity against lethal H5N1
212 influenza A viruses. Proc Natl Acad Sci U S A 107:882-7.
213 66. Kloosterman TG, Hendriksen WT, Bijlsma JJE, Bootsma HJ, van Hijum SAFT, Kok
214 J, Hermans PWM, Kuipers OP. 2006. Regulation of Glutamine and Glutamate
215 Metabolism by GlnR and GlnA in Streptococcus pneumoniae. Journal of
216 Biological Chemistry 281:25097-25109.
217 67. Härtel T, Klein M, Koedel U, Rohde M, Petruschka L, Hammerschmidt S. 2011.
218 Impact of Glutamine Transporters on Pneumococcal Fitness under Infection-
219 Related Conditions. Infection and Immunity 79:44-58.
220 68. Calder PC, Yaqoob P. 1999. Glutamine and the immune system. Amino Acids
221 17:227-41.

222 69. Castell LM, Bevan SJ, Calder P, Newsholme EA. 1994. The role of glutamine in
223 the immune system and in intestinal function in catabolic states. Amino Acids
224 7:231-43.
225 70. Newsholme P, Curi R, Gordon S, Newsholme EA. 1986. Metabolism of glucose,
226 glutamine, long-chain fatty acids and ketone bodies by murine macrophages.
227 Biochem J 239:121-5.
228 71. Newsholme P, Gordon S, Newsholme EA. 1987. Rates of utilization and fates of
229 glucose, glutamine, pyruvate, fatty acids and ketone bodies by mouse
230 macrophages. Biochem J 242:631-6.
231 72. Costa Rosa LF, Cury Y, Curi R. 1991. Hormonal control of macrophage function
232 and glutamine metabolism. Biochem Cell Biol 69:309-12.
233 73. Wallace C, Keast D. 1992. Glutamine and macrophage function. Metabolism
234 41:1016-20.
235 74. Hava DL, LeMieux J, Camilli A. 2003. From nose to lung: the regulation behind
236 Streptococcus pneumoniae virulence factors. Mol Microbiol 50:1103-10.
237 75. Marra A, Asundi J, Bartilson M, Lawson S, Fang F, Christine J, Wiesner C, Brigham
238 D, Schneider WP, Hromockyj AE. 2002. Differential fluorescence induction
239 analysis of Streptococcus pneumoniae identifies genes involved in pathogenesis.
240 Infect Immun 70:1422-33.
241 76. Obert C, Sublett J, Kaushal D, Hinojosa E, Barton T, Tuomanen EI, Orihuela CJ.
242 2006. Identification of a Candidate Streptococcus pneumoniae core genome and
243 regions of diversity correlated with invasive pneumococcal disease. Infect Immun
244 74:4766-77.

245 77. Orihuela CJ, Gao G, Francis KP, Yu J, Tuomanen EI. 2004. Tissue-specific
246 contributions of pneumococcal virulence factors to pathogenesis. J Infect Dis
247 190:1661-9.
248 78. Honsa ES, Johnson MD, Rosch JW. 2013. The roles of transition metals in the
249 physiology and pathogenesis of Streptococcus pneumoniae. Front Cell Infect
250 Microbiol 3:92.
251 79. Manzoor I, Shafeeq S, Kuipers OP. 2015. Transcriptome analysis of Streptococcus
252 pneumoniae D39 in the presence of cobalt. Genom Data 6:151-3.
253 80. van Opijnen T, Camilli A. 2012. A fine scale phenotype-genotype virulence map of
254 a bacterial pathogen. Genome Res 22:2541-51.
255 81. Mina MJ, McCullers JA, Klugman KP. 2014. Live Attenuated Influenza Vaccine
256 Enhances Colonization of Streptococcus pneumoniae and Staphylococcus aureus
257 in Mice. mBio 5:e01040-13-e01040-13.
258 82. Damjanovic D, Lai R, Jeyanathan M, Hogaboam CM, Xing Z. 2013. Marked
259 Improvement of Severe Lung Immunopathology by Influenza-Associated
260 Pneumococcal Superinfection Requires the Control of Both Bacterial Replication
261 and Host Immune Responses. The American Journal of Pathology 183:868-880.
262 83. Schmitz N, Kurrer M, Bachmann MF, Kopf M. 2005. Interleukin-1 Is Responsible
263 for Acute Lung Immunopathology but Increases Survival of Respiratory Influenza
264 Virus Infection. Journal of Virology 79:6441-6448.
265 84. Blevins LK, Wren JT, Holbrook BC, Hayward SL, Swords WE, Parks GD,
266 Alexander-Miller MA. 2014. Coinfection with Streptococcus pneumoniae

267 Negatively Modulates the Size and Composition of the Ongoing Influenza-Specific
268 CD8 ⁺ T Cell Response. The Journal of Immunology 193:5076-5087.
269 85. Shepardson KM, Larson K, Morton RV, Prigge JR, Schmidt EE, Huber VC, Rynda-
270 Apple A. 2016. Differential Type I Interferon Signaling Is a Master Regulator of
271 Susceptibility to Postinfluenza Bacterial Superinfection. mBio 7.
272 86. Nakamura S, Davis KM, Weiser JN. 2011. Synergistic stimulation of type I
273 interferons during influenza virus coinfection promotes Streptococcus pneumoniae
274 colonization in mice. Journal of Clinical Investigation 121:3657-3665.
275 87. Lee B, Robinson KM, McHugh KJ, Scheller EV, Mandalapu S, Chen C, Di YP, Clay
276 ME, Enelow RI, Dubin PJ, Alcorn JF. 2015. Influenza-induced type I interferon
277 enhances susceptibility to gram-negative and gram-positive bacterial pneumonia
278 in mice. American Journal of Physiology-Lung Cellular and Molecular Physiology
279 309:L158-L167.
280 88. Li W, Moltedo B, Moran TM. 2012. Type I Interferon Induction during Influenza
281 Virus Infection Increases Susceptibility to Secondary Streptococcus pneumoniae
282 Infection by Negative Regulation of T Cells. Journal of Virology 86:12304-12312.
283 89. Redford PS, Mayer-Barber KD, McNab FW, Stavropoulos E, Wack A, Sher A,
284 O'Garra A. 2014. Influenza A Virus Impairs Control of Mycobacterium tuberculosis
285 Coinfection Through a Type I Interferon Receptor–Dependent Pathway. The
286 Journal of Infectious Diseases 209:270-274.
287 90. Högner K, Wolff T, Pleschka S, Plog S, Gruber AD, Kalinke U, Walmrath H-D,
288 Bodner J, Gattenlöhner S, Lewe-Schlosser P, Matrosovich M, Seeger W,
289 Lohmeyer J, Herold S. 2013. Macrophage-expressed IFN-β contributes to

290 apoptotic alveolar epithelial cell injury in severe influenza virus pneumonia. PLoS
291 pathogens 9:e1003188.
292 91. van Opijnen T, Boerlijst MC, Berkhout B. 2006. Effects of random mutations in the
293 human immunodeficiency virus type 1 transcriptional promoter on viral fitness in
294 different host cell environments. J Virol 80:6678-85.
295 92. Ho SN, Hunt HD, Horton RM, Pullen JK, Pease LR. 1989. Site-directed
296 mutagenesis by overlap extension using the polymerase chain reaction. Gene
297 77:51-9.
298 93. Horton RM, Cai ZL, Ho SN, Pease LR. 1990. Gene splicing by overlap extension:
299 tailor-made genes using the polymerase chain reaction. Biotechniques 8:528-35.
300 94. Reed LJ, Muench H. 1938. A SIMPLE METHOD OF ESTIMATING FIFTY PER
301 CENT ENDPOINTS12. American Journal of Epidemiology 27:493-497.
302